Controlling the growth morphology and phase segregation of Mn-doped Ga_{2}Se_{3} on Si(001)

T. C. Lovejoy, E. N. Yitamben, S. M. Heald, F. S. Ohuchi, and M. A. Olmstead

Controlling the growth morphology and phase segregation of Mn-doped Ga$_2$Se$_3$ on Si(001)

T.C. Lovejoy,[1,][*] E.N. Yitamben,[1,][†] S. M. Heald,[2] F.S. Ohuchi,[3] and M.A. Olmstead[1]

[1]*Department of Physics, and Center for Nanotechnology (CNT),*
University of Washington, Box 351560, Seattle, Washington 98195, USA
[2]*Advanced Photon Source, Argonne National Lab, Argonne Illinois 60439, USA*
[3]*Deptartment of of Materials Science and Engineering, and Center for Nanotechnology,*
University of Washington, Box 352120, Seattle, Washington 98195, USA
(Dated: February 24, 2011)

The growth and phase segregation properties of the potential dilute magnetic semiconductor alloy, (MnSe)$_x$(Ga$_{2/3}$Se)$_{1-x}$, are studied as a function of thickness, Mn concentration, post-growth annealing, and the presence or absence of undoped Ga$_2$Se$_3$ buffer and capping layers. This system is an unusual case in heteroepitaxy where two phase MnSe+Ga$_2$Se$_3$ has better lattice matching than the (MnSe)$_x$(Ga$_{2/3}$Se)$_{1-x}$ alloy. Despite this peculiarity, this system shows a modified form of Stranski-Krastonow growth: laminar films are observed up to a certain x-dependent critical thickness, above which islands are observed by scanning tunneling microscopy (STM). The island morphology depends on the presence or absence of an undoped Ga$_2$Se$_3$ buffer layer and post-growth annealing. A kinetically stabilized platelet morphology is observed at the crossover point between laminar and islanded films. Based on Mn- and Se- K edge extended X-ray absorption fine structure (EXAFS) and X-ray absorption near edge structure (XANES), there are two types of Mn in islanded films: Mn that remains doped in the Ga$_2$Se$_3$ but oxidizes upon exposure to air, and Mn that participates in the islands, which are precipitates of the MnSe phase. Consistent with MnO or MnSe, L-edge X-ray absorption on air exposed films suggests the Mn is in the formal 2+ oxidation state. No L-edge X-ray magnetic circular dichroism (XMCD) signal is observed at 20 K, which may be due to surface effects or to a lack of magnetic order.

I. INTRODUCTION

Diluted magnetic semiconductors (DMS) that operate at high temperatures have the potential to revolutionize modern electronics, especially if they can be suitably combined with the existing technology.[1] This has led to an explosion of research in the area of DMS.[2,3] However, contradictory results by different groups on nominally identical material systems has led to an overall confusing picture of the field.[4] A critical issue in this confusion is the formation of secondary phases, whose magnetic properties can obfuscate the properties of the "true DMS" host. While being of central importance, these secondary phases are often very difficult to detect reliably,[5] and may even be caused by post-growth analysis.[6] This work studies the initial nucleation and growth of the secondary phase MnSe in Mn-doped Ga$_2$Se$_3$.

The (MnSe)$_x$(Ga$_{2/3}$Se)$_{1-x}$ alloy system is of interest as a candidate DMS by its close analogy to the prototype DMS alloy, (MnAs)$_x$(GaAs)$_{1-x}$.[7] Ga$_2$Se$_3$ is related to GaAs by the addition of one proton and electron at each anion site, and the removal of one third of cations. The resulting intrinsic vacancy material has a larger bandwidth than GaAs, which is primarily due to the vacancy-induced one-dimensional lone-pair states of Se at the valence band maximum (VBM).[8] In principle, Mn-doped Ga$_2$Se$_3$ has some advantages over Mn-doped GaAs: lattice matching allows excellent quality epitaxy on the technologically ubiquitous silicon,[9] the flexibility afforded by the intrinsic cation vacancies may allow higher Mn solubility,[10] and, unlike ferromagnetic MnAs, the secondary phase in Mn-doped Ga$_2$Se$_3$, MnSe, is antiferromagnetic.[11] Furthermore, using silicon as a substrate adds the potential to take advantage of very long spin lifetimes and transport lengths due to low spin-orbit scattering and lattice inversion symmetry.[12]

The bulk phase diagram of MnSe-Ga$_2$Se$_3$ [parameterized (MnSe)$_{3z}$(Ga$_2$Se$_3$)$_{(1-z)}$)], obtained with X-ray diffraction,[10] shows the lattice constant of Ga$_2$Se$_3$ increases with Mn concentration from 0.1 % greater than of that of Si ($a_{Ga_2Se_3} = 5.435$ Å) to about 0.6 % greater at the point where bulk MnGa$_2$Se$_4$ precipitation occurs (9 at. % Mn or $z = 0.15$). Rocksalt MnSe ($a = 5.44$ Å) has a lattice parameter intermediate between these end points with ~ 0.2 % lattice mismatch. Single phase, nearly zinc-blende, MnGa$_2$Se$_4$ ($a = 5.86$ Å) was observed in small window ($0.2 \leq z \leq 0.25$ or $11 \leq$ at. % Mn ≤ 14), before a second phase of MnSe appeared. Mixed phase MnSe and MnGa$_2$Se$_4$ were observed above $z = .25$ (14 at. %).

Neither MnSe nor MnGa$_2$Se$_4$ exhibit ferromagnetism. MnGa$_2$Se$_4$ is antiferromagnetic with a Nèel temperature of 8 K.[13] The MnSe case is more complicated; structural transitions occur simultaneously with magnetic transitions

to antiferromagnetism between 90 and 300 K.[14] The magnetism in Mn-doped layered GaSe exhibits an unusual temperature dependence where the magnetization *increases* with increasing temperature between 100 K and 170 K.[15] This is very interesting due to the possibility of a *reentrant* carrier-mediated ferromagnetic semiconductor, which becomes ferromagnetic as temperature is *increased* due the increase in free carrier density as predicted in [16] and reported experimentally in [17]. Meanwhile, nothing is known about the magnetic behavior of Mn-doped Ga_2Se_3. This raises the question of what the magnetic behavior of low concentration Mn substituting in the nearly zinc-blende Ga_2Se_3 might be. An essential first step towards possible DMS application of Mn:Ga_2Se_3 is mapping its solubility properties in thin film growth.

Contrary to the bulk phase diagram, which predicts the secondary phase $MnGa_2Se_4$, $(MnSe)_x(Ga_{2/3}Se)_{1-x}$ heteroepitaxy on Si(001):As at high x results in the secondary phase MnSe.[11] Compared to the relatively well studied A_xB_{1-x} alloys Si_xGe_{1-x} and $(InAs)_x(GaAs)_{1-x}$, $(MnSe)_x(Ga_{2/3}Se)_{1-x}$ is an unusual case in heteroepitaxy where both Ga_2Se_3 and MnSe, separately, have better lattice matching to the substrate than the alloy.

In this report, the growth and phase segregation properties of the potential DMS alloy, $(MnSe)_x(Ga_{2/3}Se)_{1-x}$, are studied as a function of thickness, Mn concentration, post-growth annealing, and the presence or absence of undoped Ga_2Se_3 buffer and capping layers. The results show some similarity to the Stranski-Krastonow growth mode that is observed for alloys with larger mismatch. For low x, about 2 atomic % Mn, laminar films are observed by scanning tunneling microscopy (STM) up to a critical thickness of ~2 nm. The critical thickness is smaller for larger x. Above the critical thickness, oriented islands with flat tops and straight edges are observed. An undoped Ga_2Se_3 buffer layer between the doped film and substrate causes the islands to be shorter and more irregular in shape than the tall islands with rectangular footprint that are observed without the buffer layer. An undoped Ga_2Se_3 overlayer has little effect on the island morphology. The pure Ga_2Se_3 morphology exhibits smooth nanoridges,[9] but the nanoridges in the laminar doped films, or in between the islands in islanded films, exhibit irregular bumps along their length that can be attributed to the presence of near surface Mn.

The atomic, electronic, and chemical structure of the films are also reported. The islands observed with STM are identified by bond length measurements from extended x-ray absorption fine structure (EXAFS) as precipitates of the rocksalt MnSe phase. Another Mn local environment, similar to MnO, observed in EXAFS is attributed to the Mn in the Ga_2Se_3 nanoridges that has been oxidized by air exposure. Based on Mn L-edge X-ray absorption for air exposed films, the Mn in the films is in the 2+ oxidation state, which is expected for either MnSe or MnO. The X-ray magnetic circular dichroism (XMCD) was also measured at the Mn L-edge for a series of samples, but no significant dichroism signal was observed. This could indicate a lack of magnetic order in Mn-doped Ga_2Se_3, but it is also possible that an intrinsic magnetic nature of these ultra-thin films is destroyed by air exposure.

II.   GROWTH AND MEASUREMENT

Preparation of quality undoped Ga_2Se_3 films by molecular beam epitaxy (MBE) on Si(001):As substrates is detailed elsewhere.[9] In brief, Si(001) is covered with a monolayer of arsenic after removal of the commercial oxide. Evaporation from a GaSe source onto a 500 °C Si(001):As substrate with flux rate of 4–8 Å/min results in a crystalline, laminar, epitaxial Ga_2Se_3 film.[8,9] These parameters are held fixed for the doping experiments. Mn is dosed with a separate Knudsen cell.

After growth, films are transferred *in-situ* in ultrahigh-vacuum (UHV) for measurement with a commercial (Omicron) UHV-STM and X-ray photoelectron spectroscopy (XPS). XPS was measured at normal emission using a Mg K_α source ($h\nu$=1253.3 eV). Immediately following growth of any of the films used in the X-ray absorption studies the XPS signal from possible trace oxygen contamination was less than the noise level in the spectra. However, while pure Ga_2Se_3 is stable against oxygen,[18] the presence of Mn greatly increases the tendency of the films to develop oxygen contamination over time, or immediately upon limited exposure to non-UHV conditions, and O 1s emission was observed on some films after STM measurements. A bright Ga LMM Auger line overlaps with the C 1s peak, so we have no information about whether there is trace carbon contamination. Droplets were observed with scanning electron microscopy on the surface of a Mn doped film and identified as gallium with energy dispersive X-ray analysis (not shown). Though significant by mass, these droplets contribute little to the XPS signal because they cover only a very small fraction of the surface. Similarly, STM measurements are conducted between these droplets, and their contribution is not observed. The droplets may be due to the growth under the selenium poor conditions used here, which is exacerbated by the addition of Mn.

Film thickness is determined in two ways (growth time and XPS); the two methods are well correlated but give very different absolute thicknesses. First, thickness is determined by separately calibrating the incident Mn and GaSe fluxes with a quartz crystal monitor (QCM) and multiplying by the deposition time. We call the thickness determined in this way the "QCM thickness" or t_{QCM}. Second, the film thickness for laminar films is measured with XPS by comparing the area under the Si 2p and Se 3d peaks utilizing Hartree-Fock photo-ionization cross sections.[19] This

gives "XPS thickness", or t_{XPS}. For laminar films, it is reasonable to expect that this procedure will give an accurate measure of the true film thickness. For islanded films, it is not possible to accurately measure film thickness with XPS. In fact, the term "thickness" is no longer well defined for islanded films. "QCM thickness" and "XPS thickness" are well correlated, but t_{QCM} is always greater than t_{XPS} due to re-evaporation during growth on a hot substrate. Empirically, $t_{XPS} \approx 0.1 \times t_{QCM} + 0.6nm$ for laminar films. The amount of re-evaporation depends sensitively on the temperature;[20] the temperature was held constant (within 10 °C) for all the doping experiments. For further details see [21].

We can also define the "QCM Mn concentration," which is almost equivalent to at. % Mn, as the amount of Mn divided by the amount of GaSe and Mn measured on the QCM. So, "QCM Mn concentration" = $Mn_{QCM}/(GaSe_{QCM}+Mn_{QCM})$. Due to the very low Mn flux for very dilute films (QCM Mn concentration less than 5%), there is a relatively large error bar in QCM measurement of the amount of Mn deposited ($\sim 30\%$).

Mn $L_{II,III}$ X-ray absorption spectra (XAS) were measured at the Advanced Light Source (ALS), beamline 6.3.1, on samples grown in Seattle. Samples were mounted with carbon tape on a copper cooling rod and mounted in the path of the X-ray beam at $\sim 10^{-6}$ torr with an incident angle 30° from grazing. The absorption was measured in total electron yield (TEY) and normalized by the TEY from a gold mesh upstream of the sample. Due to the absence of a reliable calibration in this energy range, spectra were aligned in energy manually.

X-ray magnetic circular dichrosim (XMCD) was conducted. Slits were used to select a section of the beam with ~ 60 % circular polarization. A magnetic field was applied parallel to the beam direction by an electromagnet outside the vacuum system. The applied field was alternated at each photon energy between positive and negative 2,000 Oe. The dichroism spectra were then computed by taking the difference between the plus and minus field data at each point divided by their sum (not shown).

Samples grown and checked in UHV with STM and XPS were measured in air for K-edge X-ray absorption measurements at the Advanced Photon Source (APS) sector 20BM PNC/XOR-CAT. The incident beam intensity was measured with an ionization chamber before the sample for normalization. Samples were mounted on spinners and rotated about the sample normal at about 3 Hz during measurement where X-rays polarized near the plane of the sample impinged at grazing incidence ($2 - 3°$). The X-ray energy was scanned through the Mn, Se, and Ga K-edge energies, and the K-edge fluorescence was captured from near the plane of the sample ($\sim 5°$) with a liquid nitrogen cooled, thirteen element Ge detector. For the MnSe and Ga_2Se_3 reference samples, commercial powders (ESPI metals) were ground to a very fine powder and spread onto tape. The absorption due to the reference samples was measured in transmission with an ionization chamber downstream of the sample. For both the reference and thin film samples, a small amount of the beam continued downsteam of the sample and passed through a standard reference sample followed by an additional ionization chamber to measure the edge position of the standard reference sample in transmission. This allowed for an accurate determination of the absolute beam energy because the edge position of the standard reference sample is known. Background subtraction, normalization, and Fourier transforms were done in the standard way using the Athena computer program.[22]

III. RESULTS

Figure 1 summarizes the series of films that were grown in terms of thickness and concentration, and groups the films into three categories: laminar, platelet, and islanded. This grouping is determined by STM, as described in the next section. The labels on the samples in Fig. 1 are used throughout this article to identify the various samples. For some films, the Mn-doped films were grown directly on Si(001):As – referred to below as "direct" films. For other films, an undoped Ga_2Se_3 layer was deposited first on Si(001):As, and then the Mn-doped film was grown on top of that with the thickness and Mn concentration given – referred to below as "buffer layer films". The buffer layer used had a QCM thickness of ~ 3 nm except for the following: B1, 9 nm; B9, 4 nm; B6, 1 nm; B2, 2 nm. For some films, an undoped Ga_2Se_3 layer with QCM thickness ~ 3nm was deposited on top of the direct Mn-doped film – referred to below as "overlayer" films. Recall that "QCM thickness" is an overestimate of the true thickness (by up to 5 times) due to reevaporation during growth.

A. Surface and Island Morphology (STM)

The film morphology for dilute Mn-doped Ga_2Se_3 films grown on Si(001):As depends on film thickness. Figure 2 (a)–(c) shows the film morphology for direct films with QCM Mn concentration ~ 2 % as a function of increasing QCM thickness from 3 nm to 15 nm. For undoped films the only morphological change in this thickness range is that the nanoridges become wider; under these Se-poor conditions, layered GaSe begins to form at much higher thicknesses.[20] The morphology in Fig. 2 (a, D1), for a film with $t_{QCM} \sim 3.4$ nm, is characterized by long "nanoridges" aligned

along Si[110]. This nanoridge morphology is similar to that reported previously for pure Ga_2Se_3 on Si(001):As, and is understood to result from ordering of the intrinsic vacancies.[9] The long directions of the nanoridges are aligned with the dimer rows of the well-known Si(001) 2×1 reconstruction.[20] The dimer rows, and thus the nanoridges, rotate 90° with each quarter-unit-cell step between terraces on the substrate. To emphasize the relationship between the dimer rows of the substrate and the orientation of the nanoridges, the film shown in Fig. 2 (a, D1) was grown on a substrate with 4° miscut, which is known to result in half-unit-cell steps between terraces and only a single orientation of the dimer rows. As a result, all the "nanoridges" are aligned parallel to each other, whereas for a substrate with no miscut, two orientations of nanoridges are observed.[8,9]

The nanoridge morphology persists up to a QCM thickness of about 10 nm, at which point a new morphology is observed. This new morphology, shown in Fig. 2 (b, D5), consists of occasional tall islands surrounded by a mixture of relatively wide, flat platelets and nanoridges. This platelet morphology is only observed in a narrow thickness range between 10 and 15 nm, and in this range the morphology depends sensitively on preparation conditions. That is, films with very similar thickness and Mn concentration exhibit different morphologies. This is shown in Fig. 1 at the 10 nm side by distinction between D4 (not shown) and D5. The former has a laminar morphology similar to that shown in Fig. 2 (a, D1), while the latter takes the platelet morphology (Fig. 2 (b, D5)). Also, at the 15 nm side, two films, D6 and D7, very nearby in Fig. 1 have very different morphology. The morphology of D6 resembles the platelet morphology of D5 (see Fig. 5 (a, D6)), while D7 takes a highly islanded morphology (Fig. 2 (c)).

The highly islanded morphology of the film shown in Fig. 2 (c, D7) is characterized by 6–8 nm tall islands with rectangular footprints. The island edges are oriented along the Si[110] or Si[1$\bar{1}$0]. Typical lateral dimensions are 20–100 nm. Most islands have a long direction and short direction, with the long direction being 2–5 times longer. The identical "flower" shape of the tallest islands in Fig. 2 (c, D7) is an experimental artifact due to tunneling to the sides of STM tip, which also makes it difficult to get high quality images of the small flat regions in between the islands.

At higher Mn concentrations, islands are observed even for very thin films, and the island morphology depends on the presence or absence of an undoped Ga_2Se_3 buffer layer. Figure 3 compares the morphology between two films, a direct film and a buffer layer film, with similar Mn concentration (QCM Mn Con. ∼8%). Both doped films have a QCM thickness of ∼3 nm. The direct film morphology, (a, D8), is characterized by 2–4 nm tall islands with flat tops and rectangular foot print. In between the islands there is a flat film with the nanoridge morphology of undoped Ga_2Se_3. Similar to the highly islanded morphology of Fig. 2 (c, D7), the island edges are aligned parallel to Si[110] or Si[1$\bar{1}$0], and most islands have a long direction 3–5 times longer than short direction.

In the buffer layer case (Fig. 3 (b, B4)) the islands are shorter and more irregular in shape. In our previous report,[11] we showed STM data from a similar sample (B5). For completeness, those results are restated here. On the terraces between the islands there is a nanoridge morphology with wider nanoridges and larger height variation than the undoped case. The island perimeters are locally aligned with the nanoridge morphology. Though irregular, the islands tend to be elongated along the same direction as the long-axis of the nanoridges. As with the dimer rows of the substrate and the nanoridges, the long direction of the film's island morphology rotates 90°at each substrate step. Some islands cross substrate steps, resulting in "L" or "T" shaped intersections, which contribute to the irregularity of the island shapes. Some islands have an incomplete top layer covering 10% to 90% of the island; the step height from this layer to the next is ∼ 2.7 Å.

STM of Mn doped films shows small (∼ 0.5 Å) apparent protrusions (bumps) along otherwise smooth nanoridges. To isolate the effect of Mn on the nanoridge morphology, 0.6 Å Mn was deposited on pure Ga_2Se_3 at the standard growth temperature, 500 °C. Before Mn deposition (Fig. 4 (a) and (a′)) the nanoridges are relatively smooth, with corrugation below 0.1 Å. After Mn deposition (Fig. 4 (b, P2+Mn)) the rods exhibit randomly spaced bumps along their length. The bumps are ∼2 nm wide and typically ∼0.5 Å "tall". For an islanded film like that shown in Fig. 3 (b, B4), the nanoridges in between islands also exhibit bumps along their length. The bumps in this case are ∼1 nm wide and ∼0.5 Å "tall". This is shown in Fig. 4 (c, B3). The nanoridges for laminar Mn-doped films exhibit similar bumps along their length (not shown). These protrusions appear to be due to the presence of Mn near the surface of the nanoridges.

The platelet morphology of Fig. 2 (b) also exhibits nanoridges on the tops of the platelets, but their morphology is distinctly different from that of pure Ga_2Se_3 and the other Mn-doped morphologies. Figure 5 (a, D6) shows the morphology of another film with the platelet morphology. Whereas the nanoridges of the pure Ga_2Se_3 morphology exhibit a range of spacings and heights, the nanoridges of the platelet morphology are all equal in height and regularly spaced (∼2.8 nm). Groups of 10–30 rods appear as platelets ∼30–90nm wide and up to 70 nm long in Fig. 5 (a, D6). An expanded view of one platelet is shown in Fig. 5 (a inset, D6). In between the platelets, there are also nanoridges at various heights with varied spacing, similar to the undoped Ga_2Se_3 morphology.

The platelet morphology of Figs. 2 (b, D5) and 5 (a, D6) is metastable with respect to annealing. Figure 5 (b, D6A) shows the film from Fig. 5 (a, D6) after annealing for 30 minutes at 500 °C—the same temperature as for growth. The post-annealing morphology is distinctly different. Nothing remains of the platelet morphology, and there

are now much larger islands with flat tops and irregular shapes. These islands have heights from 3 nm to 6 nm and cover a large fraction of the surface. The relatively flat regions resemble a somewhat disordered version of the pure Ga_2Se_3 nanoridge morphology, similar to the terrace regions of the higher concentration buffer layer film shown in Fig. 3 (b, B4).

Depositing an undoped Ga_2Se_3 overlayer has little effect on the film morphology. For example, the morphology of the sample in Fig. 3 (a, D8) was also observed after depositing an overlayer (not shown), and the result was essentially indistinguishable from the morphology beforehand. Specifically, the morphology was still characterized by tall islands with rectangular foot prints sticking out from a layer with the nanoridge morphology of pure Ga_2Se_3. This is different from the case of Cr-doping of Ga_2Se_3 where islanding is also observed, but where an undoped overlayer has a dramatic effect in reducing the size of the islands.[23]

B. Electronic Structure: Mn L-edge, Mn 2p

Excitation of the Mn $2p$ core level via X-ray photoemission and absorption yields sensitive, atom-specific information about the local electronic and magnetic structure.

Mn L-edge XAS of air exposed films closely resembles the result expected for atomic Mn in the 2+ (d^5) oxidation state. Fig. 6 (a) shows the strong similarity in XAS for two films: one with the platelet morphology (D5, see Fig. 2 (b)), and one with an islanded morphology (B6), scaled to the same maximum intensity. The spectra overlap closely. XAS from laminar films (D2, D3) and an islanded film with higher Mn concentration (B2) also overlap closely with the spectra shown in Fig. 6 (a), except for small variations in the background. These spectra resemble the computed result for atomic Mn in the 2+ (d^5) oxidation state with zero crystal field shown in Ref. 24. The spectra also resemble the XAS for air exposed films of Mn-doped GaAs.[25]

Any dichroism signal from XMCD at 20 K was less than 1 % for all of the samples measured (P3, D5, D3, B2, D2), which is comparable to the noise level in the spectra.

Mn $2p$ XPS was measured *in situ* using Mn K_α radiation (1253.6 eV); the spectra include the overlapping contribution of the Mn LMM Auger peak. Figure 6 (b) shows the Mn $2p$ XPS peaks for Mn metal deposited directly on Si(001):As, and two Mn-doped Ga_2Se_3 films (D6 and D6A). The spectra are normalized to the height of the Mn $2p_{3/2}$ peak. For the Mn metal three features are observed: Mn $2p_{3/2}$ (~ -639 eV), Mn $2p_{1/2}$ (~ -650 eV), and the Mn LMM Auger (KE$\sim$ 588 eV or BE~ -665 eV). The overall shape of the Mn $2p$ peak in the Mn-doped Ga_2Se_3 films is similar between films with different morphology, but quite different from the single component metallic line shape for Mn metal. The doped-film emission is broader, shifted to higher binding energy (BE ~ -641 eV), and exhibits "satellite" structures on the low kinetic energy side of the Mn $2p_{3/2}$ and Mn $2p_{1/2}$ peaks, labeled "s" in Fig. 6 (b). Also, the LMM Auger line is significantly more intense relative to the Mn $2p_{3/2}$ peak. Figure 6 (b) shows the Mn 2p for two representative and easily comparable cases: a platelet morphology film, see Fig. 5 (a); and for the same platelet morphology film after a post-growth anneal changed the morphology to an islanded type, see Fig. 5 (b). The shape of these two spectra are quite similar, but the relative intensity of the Mn LMM Auger peak to the Mn 2p photoemission peak is greater in the annealed, islanded film. Mn 2p peaks were measured on most of the films in Fig. 1, and regardless of morphology, all have similar shape to these two cases, except for some variation in the relative intensity of the LMM Auger peak, and in the intensity of the Auger feature centered at binding energy -632 eV (KE$\sim$621 eV). The spectra are flat in the regions of the two Auger features when using a different photon energy, but the satellite features remain.

C. K-edge X-ray absorption

Clear information about the local bonding environments of each atomic species can be extracted from K-edge X-ray absorption.

Figure 7 shows the Mn K edge XANES for a MnO reference powder, a laminar Mn-doped film (D3), an islanded direct film (D7), an islanded buffer layer film (B8), and a MnSe reference powder. The position of the absorption edge shifts monotonically to lower photon energy through this series for a total shift of about -2.5 eV between MnO and MnSe. Because Se and O occupy the same column on the periodic table, we expect the Mn in MnSe or MnO to be in the formal 2+ oxidation state.

Se K-edge EXAFS were measured on a Ga_2Se_3 powder, an undoped Ga_2Se_3 film (P3), a laminar Mn-doped Ga_2Se_3 film (D3), an islanded direct film (D7), an islanded buffer layer film (B8), and a MnSe powder. Figure 8 shows k^2 weighted $\chi(k)$ data in (a), and the magnitude of its Fourier transform, $|\chi(R)|$, in (b) for each Se K-edge. The $\chi(k)$ data for the Ga_2Se_3 powder, the undoped film, and the laminar doped film each consist of simple oscillations with approximately equal spacing. This leads to the relatively simple $|\chi(R)|$ plots where the dominant feature is a single

peak just above R = 2 Å corresponding to a single first neighbor bond length around 2.4 Å. The absence of second neighbor peaks (R∼3–4 Å) in $|\chi(R)|$ in Ga_2Se_3 reference materials has been reported previously,[26] and has been attributed to the increased disorder in the bond lengths due to the intrinsic vacancies. The MnSe reference sample, on the other hand, shows both a clear first neighbor peak at R ∼2.3 Å, corresponding to a first neighbor bond length of about 2.7 Å, and second neighbor peak at R∼3.5 Å, corresponding to a second neighbor bond length of about 3.8 Å. The data for the islanded samples, B8 and D7, is more complex due to the overlapping contributions of several bonds with similar lengths.

The results of fits to the Se EXAFS data using FEFF6[27] are shown in Fig. 8 (a) and (b). Each data set was fit separately assuming certain scattering paths with neighbor species and initial bond lengths corresponding to known phases. For the selenium K edge, paths were selected from among oxygen first-neighbors in selenium oxide, Ga first-neighbors in Ga_2Se_3, and Mn first- and Se second-neighbors in MnSe. Paths were excluded if they did not improve the quality of the fit. Table I shows which paths were included for fitting each data set, which fit parameters were used, and the values from the fit. For data fit with first and second neighbor paths, the k and R ranges were 2–13 Å^{-1} and 1–4 Å, respectively, or slightly wider for the reference samples. If only first neighbor paths were included, the k and R ranges were 2–10 Å^{-1} and 1–3 Å. As shown in Table I, depending on whether 1, 2, or 4 paths were included, the total number of fit parameters was either 4, 5, or 11, respectively.

Figure 9 (a) shows k^2 weighted $\chi(k)$ Mn K-edge EXAFS for a Mn-doped laminar film, a Mn-doped islanded direct film (D7), a Mn-doped islanded buffer layer film (B8), and powdered MnSe; $|\chi(R)|$ is in Fig. 9 (b). The peak in $|\chi(R)|$ around 1.5 Å corresponds to manganese oxide first neighbor bonds, and the peaks around 2.5 Å and 3.5 Å can be related to first (bond length = $a/2$ = 2.72 Å) and second neighbor bonds (bond length = $\sqrt{2} \times a/2$ = 3.82 Å) in rocksalt MnSe, respectively. To fit the Mn K-edge, scattering paths were selected from among oxygen first-neighbors in manganese oxide, and Mn first- and Se second-neighbors in MnSe. The results of the FEFF6 fits are shown in Fig. 9 (a) and (b), and the fit parameters are reported in Table I. When only the first neighbor oxide path was included, the k and R ranges were 2–5.8 Å^{-1} and 1–3 Å, respectively. Otherwise, they were 2–13 Å^{-1} and 1–4 Å (or slightly wider for the reference sample). As shown in Table I, depending on whether 1, 2, or 3 paths were needed, the total number of fit parameters was either 4, 5, or 8.

Ga K-edge EXAFS of powdered Ga_2Se_3 shows a first neighbor bond at 2.43 Å, within error bars of the same bond measured with Se EXAFS. Thin film data are dominated by a much shorter first neighbor bond length of ∼ 1.92 Å, which corresponds to gallium oxide. (Ga K edge data not shown)

IV. DISCUSSION

The electronic structure, atomic structure, and growth properties of Mn-doped Ga_2Se_3 films have been studied as function of Mn concentration, thickness, post-growth annealing, and buffer/capping layers. Figure 1, a "QCM Mn concentration" versus "QCM thickness" scatter plot, serves as a sample index for cross-referencing the information about electronic and atomic structure from XPS and X-ray absorption data with the morphology observed with STM.

A. Surface Morphology

All the films are loosely grouped into three categories based on their morphology from STM: "laminar", "islanded," and "platelet." "Laminar" films (i.e. Fig. 2 (a, D1)) have a nanoridge morphology similar to pure Ga_2Se_3 with total corrugation less than 0.5 nm. "Islanded" films have a large fraction of the surface covered with islands taller than 1 nm. The islands protrude from flat terraces with a nanoridge morphology similar to the "laminar" morphology; the specific island morphology can be varied significantly by changing the growth parameters (e.g. Fig. 2 (c, D7), Fig. 3 (a, D8) and Fig. 5 (b, D6)). "Platelet" films (e.g. Fig. 2 (b, D5) and Fig. 5 (a, D6A)) have a small number of islands 1–2 nm tall surrounded by laminar terraces consisting of platelets and nanoridges.

The nanoridges in doped films, whether in laminar films or in the inter-island regions in island films, are similar in overall morphology to undoped Ga_2Se_3 films, but different at the atomic scale. As shown in Fig. 4, the nanoridges in doped films exhibit bumps along their length that are not observed without Mn. These bumps are attributed to the changes in electronic states brought about from presence of Mn near the surface of the nanoridges.

The platelet morphology exhibits large atomically smooth "platelets," which is different from laminar films and the inter-island regions in islanded films where Ga_2Se_3 nanoridges grow on top of each other to various heights, creating a comparably rough surface. The regularly spaced nanoridges that make up the platelets exhibit a period (2.8 nm) that is much larger than any typical unit cell. This different morphology may indicate that the platelets take a different structure than the islands or nanoridges. The regularly spaced, large period, ridges may be due to lattice dislocations

caused by a lattice mismatch. The platelets may take the MnGa$_2$Se$_4$ phase (mismatch $\sim$ 8 %), which would be consistent with the bulk phase diagram for this system, and could explain the dislocations.

Despite the difference in structure, the platelet films and islanded films show similar local Mn environments. The Mn $L_{II,III}$ edge XAS is very similar between islanded and platelet films (Fig. 6 (a)). Also, the Mn 2p XPS peaks of platelet and islanded films are quite similar, except for minor variations in the relative intensity of the Mn LMM Auger and the Auger feature at -632 eV. See Fig. 6 (b). The high binding energy satellite features observed in both cases are often observed in the core level photoemission from Mn in semiconducting or insulating compounds. They can be interpreted using the configuration-interaction scheme as arising from the overlapping contributions of different possible final states. See Refs. 28 and 29. The differences in intensity of the Auger features may be due to differences in the available final states between the platelet and islanded films, which could also explain why the Auger feature at -632 eV is not observed in the electronically very dissimilar Mn metal. Increased inelastic scattering from the taller islands could also lead to an apparent increase in Auger intensity.

The platelet morphology is kinetically-stabilized, and has a sensitive dependence of the growth parameters. Comparison of the morphology of a platelet film before and after annealing, Fig. 5 (a) and (b), shows that the platelet morphology is metastable with respect to annealing at the growth temperature. This suggests that the platelet morphology is kinetically stabilized and that the highly islanded morphology is the energetically favorable one. This also implies a sensitivity to the rate of temperature decrease after the growth is stopped. This sensitivity, together with limited reproducibility in the cooling rate, may explain why samples with similar Mn concentration and thickness (i.e. D4/D5 or D6/D7 in Fig. 1) exhibit different morphology.

Kinetically stabilized phases are of general interest due to the possibility of creating useful meta-stable systems, which might be far from energetically stable. Low temperature (LT) MBE grown (MnAs)$_x$(GaAs)$_{1-x}$ is a relevant example of a kinetically stabilized phase. LT-MBE (MnAs)$_x$(GaAs)$_{1-x}$, together with post growth annealing treatments, result in Mn incorporation at concentrations far above the bulk solubility limit.[30] These elaborate growth sequences have generated steadily increasing magnetic transition temperatures. Future development of growth and post-growth techniques may allow thicker laminar (MnSe)$_x$(Ga$_{2/3}$Se)$_{1-x}$ with higher Mn concentrations. However, simply decreasing the growth temperature does not work for the Se-poor conditions used here because the layered GaSe phase becomes dominant at lower temperatures.

B. Correlation of electronic and atomic structure with morphology

L- and K-edge X-ray absorption yields clear information about the local bonding environments of each atomic species. By comparing with the known local environments of various bulk Mn-Ga-Se phases, it is possible to identify which phases are present in the thin film samples.

The local bonding environments of the Mn and Se suggest the presence of different phases in the islanded films (MnSe, Ga$_2$Se$_3$, oxides) than in the laminar films (Ga$_2$Se$_3$, oxides). The local environments of the Se in the undoped Ga$_2$Se$_3$ film and laminar Mn-doped film are similar to the Ga$_2$Se$_3$ reference sample. As shown in Table I, the undoped film has a slightly shorter Se-Ga bond length ($\sim$2.34 Å) than the reference powder ($\sim$2.40 Å), and is closer to the 2.36 Å spacing expected for the ideal zinc-blende structure. For the laminar Mn-doped film, the Se-Ga bond length ($\sim$2.41 Å) is closer to the reference sample. This may be due to Mn incorporation increasing the lattice constant. Based on the Mn K-edge data, the Mn in the laminar Mn-doped film participates primarily in manganese oxide (bond length $\sim$2.12 Å). For Mn substitution on a Ga site in Ga$_2$Se$_3$, we would expect a bond length around 2.4 Å (same as Se-Ga bond length), but this is not observed. The local environments of the Se and Mn in islanded films indicate the presence of Ga$_2$Se$_3$ and MnSe phases as well as oxides. From the fitting of the Se K-edge EXAFS for the islanded films B8 and D7, both Mn first neighbors (bond length 2.70 Å) and Se second neighbors (bond length 3.81 Å) are observed corresponding to the MnSe phase. The Se also participates in the Ga$_2$Se$_3$ phase with bond length $\sim$2.37 Å, and an oxide phase with bond length $\sim$1.5 Å. The Mn K-edge supports the MnSe phase identification in the islanded films because consistent Se first neighbor bond lengths (2.72 Å (D7) and 2.70 Å (B8)) and Mn second neighbor bond lengths ($\sim$3.8 Å) are observed. See Table I. Similar to the Mn in the laminar doped film, the Mn in the islanded films also participates in manganese oxide with a bond length of about 2.15 Å. Again, we do not observe the 2.4 Å bond length that would be expected for Mn substitution on a Ga site. These results expand on our previous report,[11] which showed data only from an islanded buffer layer film, by showing that the crystallographic phase of the islands does not depend on the presence of the buffer layer, and laminar film data.

The Mn K-edge XANES can sometimes be used as fingerprint for certain types of chemical bonding.[31] In this case, the gradual shift in position and shape of the Mn XANES (see Fig. 7) can be used to rank the relative oxidation of the different samples. The edge position shifts between MnO and MnSe, which is probably due to the Mn-O bond being more ionic in nature than the Mn-Se bond. The gradual shift in the edge position of the thin film samples can be understood in terms of an decreasing degree of oxidation from the laminar doped film (D3), to the islanded direct

film (D7), to the islanded buffer layer film (B8). This is consistent with the trend from the EXAFS result. See, for example, the $|\chi(R)|$ plot in Fig. 9 (b), which shows decreasing weight at the Mn-O bond (R$\sim$1.5 Å) along the same series of samples. This leads to the conclusion that the Mn in the laminar film is more prone to oxidation.

By correlating STM results with K-edge EXAFS and XANES for the various samples, we propose that there are two types of Mn in islanded Mn-doped Ga_2Se_3 films: Mn that participates in phase-separated islands of the MnSe phase, and Mn that remains doped in the Ga_2Se_3, but floats to the surface during growth. The existence of the MnSe phase is well supported in the islanded films by the observation of the corresponding first and second neighbor bond lengths for both Mn and Se. As discussed in our previous report, the step heights of incomplete island layers (~ 2.7 Å) from STM in a buffer layer film also supports the MnSe phase identification and suggests a specific epitaxial orientation with the substrate.[11] The orientation of the island perimeters (aligned with Ga_2Se_3 nanoridges) suggests a similar epitaxial orientation for the MnSe islands in the direct case. A schematic view of this epitaxial alignment is shown in Fig. 10.

The second type of Mn in doped films, the Mn that does not participate in MnSe islands, is observed by STM as bumps along the nanoridges of the Ga_2Se_3 morphology. As STM is extremely surface sensitive, the Mn thus observed must be very near the surface. An oxidized Mn component is observed in air exposed films by EXAFS and XANES. Given that the Mn was not oxidized before air exposure, as determined by XPS, it is reasonable to expect that the Mn observed on the surface by STM is oxidized by air exposure. So, it is consistent to assign the oxidized Mn component observed in the K-edge data as that Mn which remained in the Ga_2Se_3 film. This assignment is supported by the inverse correlation between islanding observed by STM and oxidation observed by EXAFS and XANES. That is, the non-islanded film (D3) is the most oxidized, and the most highly islanded film (B8) is the least oxidized.

We interpret observation of a single gallium oxide bond in the K-edge EXAFS from the thin film samples as being due to the formation of gallium droplets during growth and subsequent oxidization upon exposure to air. While having little effect on the STM or XPS data, sparse Ga droplets would dominate the signal in the bulk sensitive EXAFS experiments.

The L- and K-edge XAS and Mn 2p photoemission indicate that the Mn is in the formal 2+ (d^5) oxidation state regardless of growth conditions. EXAFS at the K-edge shows that Mn participates either in MnO or MnSe-like phases; in either case, we would expect Mn to be in the formal 2+ oxidation state.

There are several similarities between the island growth observed in $(MnSe)_x(Ga_{2/3}Se)_{1-x}$ and that observed in Si_xGe_{1-x} and $(InAs)_x(GaAs)_{1-x}$. For example, the transition from laminar to islanded growth can be described in all three systems in terms of laminar films up to some critical thickness, at which point islands begin to nucleate and grow. Furthermore, the critical thickness for island formation depends on the alloy concentration in each case; higher x leads to a lower critical thickness. See Ref. 32, and the references therein. As shown in Figs. 1 and 2, for 2 at.% Mn, the transition from laminar to islanded growth occurs in the range of QCM thickness between $10-15$ nm (XPS thickness $1.6-2.1$ nm). The dependence of the critical thickness on Mn concentration is easily seen by comparing Fig. 2 (a, D1), with QCM Mn concentration $\sim$2%, and Fig. 3 (a, D8), with QCM Mn concentration $\sim$6%. Both films have a QCM thickness of ~ 3 nm (XPS thickness ~ 1 nm), but the film with higher Mn concentration exhibits an islanded morphology.

These commonalities are very interesting because the interaction between strain and phase segregation is opposite between $(MnSe)_x(Ga_{2/3}Se)_{1-x}$ and Si_xGe_{1-x} or $(InAs)_x(GaAs)_{1-x}$. That is, strain generally works against phase segregation in Si_xGe_{1-x} and $(InAs)_x(GaAs)_{1-x}$, yet it appears to be the driving force behind the MnSe phase segregation in $(MnSe)_x(Ga_{2/3}Se)_{1-x}$ on Si(001):As.

Adding an undoped Ga_2Se_3 buffer layer between the Si(001):As and the doped film still results in an islanded morphology, but the islands are much shorter and cover a larger fraction of the surface. (Fig. 3 (b)). The difference in island morphology between films with and without a buffer layer (Fig. 3) may be attributed to the undoped Ga_2Se_3 buffer layer preventing reaction of the Mn with the As monolayer. Ga_2Se_3 has been shown to be an effective buffer layer against oxidation of Si(001):As,[18] and it is reasonable to assume that it could also serve to buffer Mn from interacting with Si(001):As. The Mn-As bond length is longer than the Mn-Se bond length, and Mn-As bonding could provide local strain centers. Islands with smaller footprints minimise interface strain energy more than islands with large footprints because strain energy increases with interface area. This may explain why the islands have smaller footprints when no buffer layer is used. MnSe islands in the buffer layer case have relatively little mismatch strain because the lattice mismatch between MnSe and Ga_2Se_3/Si is small ($\sim$0.2%), which may lead to the comparably large footprints.

When the growth order is reversed (an undoped Ga_2Se_3 overlayer is grown on top of the direct film) little change in the island morphology is observed. This suggests that island morphology does not depend sensitively on the Mn chemical potential. One might expect the Mn in the islands to partially dissolve into the Ga_2Se_3 film as more Ga_2Se_3 material was added. The morphology of the Cr-rich islands in Cr-doped Ga_2Se_3 are greatly affected by a Ga_2Se_3 overlayer, which has been attributed to a reversal of the Cr chemical-potential gradient and subsequent dissolution of the islands.[23] This does not occur in Mn-doped Ga_2Se_3, which is consistent with MnSe islands that are energetically

and kinetically stable. Also, Ga_2Se_3 overlayers may be useful for preventing the oxidation of the films for *ex-situ* magnetic or device measurements.

The very small or absent dichroism signal in air exposed films at the Mn $L_{II,III}$ edge in air exposed films may suggest a lack of ferromagnetic ordering in Mn-doped Ga_2Se_3, but it is also possible that the films exhibit magnetic order that is not seen in XMCD due to surface effects. The most closely analogous system, Mn-doped GaAs, shows an XMCD signal around 40% under similar measurement conditions (15 K, 85% circular polarization, ±0.6 T).[25] Neglecting surface effects, the maximum XMCD signal would be somewhat smaller for our measurements due to the lower degree of circular polarization of the light ($\sim60\%$) and smaller applied field (±0.2 T) leading to the possibility of measurement under non-saturated conditions. In the Mn-doped GaAs case, XMCD and XAS studies before and after HCl etching revealed a surface layer with very different electronic and magnetic structure. Similar to our observation, this surface layer showed pronounced atomic multiplet structure and little dichroism.[25] It is not possible to treat the very thin laminar films grown here with HCl surface cleaning because Mn-doped films are dissolved by water. As was initially the case for Mn-doped GaAs, some form of more elaborate growth (i.e. LT-MBE) or post-growth (i.e. surface capping or etching) technique may prove necessary to elucidate the magnetic nature of the Mn:Ga_2Se_3 system.

Controlling the self assembly and subsequent growth morphology, especially the size and ordering, of nanostructures is a major goal for the advancement of nanotechnology.[33–35] This work demonstrates a high degree of control over the morphology of MnSe nanostructures by tuning the phase segregation properties in $(MnSe)_x(Ga_{2/3}Se)_{1-x}$. The parameters that control the nanostructure (island) morphology include the amount of material deposited ("thickness"), the presence or absence of undoped Ga_2Se_3 buffer layers, and post growth annealing. The resultant MnSe nanoparticles have lateral dimensions in the range of 10–50 nm, with heights between 2 and 6 nm. Accessible nanoparticle shapes include regular shapes with rectangular footprints to highly irregular shapes involving "T" and "L" shaped intersections. The anisotropy of the nanostructures can also be varied with length/width values ranging from about 100 for the doped nanoridges in the laminar films to about 2 for the regular island shapes observed for direct films. This nano-scale synthesis route could complement the recently developed solution chemistry synthesis route to achieving micro-scale MnSe particles.[36]

V.   CONCLUSION

Laminar Mn-doped films Ga_2Se_3 grow below a certain critical thickness, and the critical thickness is smaller for higher Mn concentrations. For thicker or more concentrated films, islands are observed. A kinetically-stabilized platelet morphology is observed at the cross over point from laminar to islanded for low x. Despite the better lattice matching of phase separated MnSe+Ga_2Se_3 to the substrate for $(MnSe)_x(Ga_{2/3}Se)_{1-x}$ heteroepitaxy on Si(001):As, this is qualitatively similar to the Stranski-Krastanov growth mode observed in the more studied compounds like Si_xGe_{1-x} and $(InAs)_x(GaAs)_{1-x}$where strain works against phase segregation. Upon annealing, this morphology changes to a morphology more closely resembling the high x buffer layer morphology. At high x the dependence of the island morphology on the presence or absence of an undoped Ga_2Se_3 buffer layer is interpreted as resulting from whether or not the Mn can react with the arsenic surfactant monolayer – that reaction being inhibited in the buffer layer case. The island morphology is not significantly affected by an undoped overlayer, which suggests that the islands are stable with respect to small changes in the Mn-chemical potential.

Bond length measurements for K edge EXAFS on air-exposed films reveal the presence of MnSe and manganese oxide bonds in islanded films, but only manganese oxide in laminar films. So, in contradiction with the bulk phase diagram, which predicts the formation of $MnGa_2Se_4$ precipitates, the islands observed with STM are identified as precipitates of the rocksalt MnSe phase. The difference from the bulk case is probably due to the superior lattice matching of the phase MnSe to silicon compared to $MnGa_2Se_4$.[11] The platelets in the platelet morphology films may take the $MnGa_2Se_4$ phase. Because the Mn was not oxidized during growth, as determined by XPS, the manganese oxide component is attributed to Mn that remained doped into the Ga_2Se_3 nanoridges, where it was observed as bumps with STM, but was oxidized by exposure to air before the EXAFS was measured. This model is consistent with the Mn K-edge XANES, which also shows increasing oxidation of the Mn for more laminar films. For laminar and islanded films, the Mn L-edge absorption suggests the Mn is in the 2+ oxidation state, which is expected for either MnSe or MnO, and no significant dichroism is observed in XMCD. This may imply a lack of magnetic order, or simply that the films are too thin and reactive to survive air exposure without a more sophisticated method of surface protection. Thicker films may still be of interest for DMS applications, particularly if low temperature growth of $(MnSe)_x(Ga_{2/3}Se)_{1-x}$ can be achieved.

Acknowledgments

* Electronic address: `tlovejoy@uw.edu`

† Current Address: Center for Nanoscale Materials, Argonne National Laboratory, Argonne, Illinois 60439, USA

[1] S. Wolf, D. Awschalom, R. Buhrman, J. Daughton, S. Von Molnar, M. Roukes, A. Chtchelkanova, and D. Treger, Science **294**, 1488 (2001).

[2] S. Koshihara, A. Oiwa, M. Hirasawa, S. Katsumoto, Y. Iye, C. Urano, H. Takagi, and H. Munekata, Phys. Rev. Lett. **78**, 4617 (1997).

[3] H. Ohno, D. Chiba, F. Matsukura, T. Omiya, E. Abe, T. Dietl, Y. Ohno, and K. Ohtani, Nature **408**, 944 (2000).

[4] S. A. Chambers, Surf. Sci. Rep. **61**, 345 (2006).

[5] T. C. Kaspar, T. Droubay, S. M. Heald, M. H. Engelhard, P. Nachimuthu, and S. A. Chambers, Phys. Rev. B **77**, 201303 (2008).

[6] M. A. White, T. C. Lovejoy, S. T. Ochsenbein, M. A. Olmstead, and D. R. Gamelin, J. Appl. Phys. **107**, 103917 (2010).

[7] H. Ohno, Science **281**, 951 (1998).

[8] T. C. Lovejoy, E. N. Yitamben, T. Ohta, S. C. Fain, F. S. Ohuchi, and M. A. Olmstead, Phys. Rev. B **81**, 245313 (2010).

[9] T. Ohta, D. A. Schmidt, S. Meng, A. Klust, A. Bostwick, Q. Yu, M. A. Olmstead, and F. S. Ohuchi, Phys. Rev. Lett. **94**, 116102 (2005).

[10] M. Quintero and J. C. Woolley, Phys. Stat. Sol. (a) **141**, 53 (1994).

[11] T. C. Lovejoy, E. N. Yitamben, S. M. Heald, F. S. Ohuchi, and M. A. Olmstead, Appl. Phys. Lett. **95**, 241907 (2009).

[12] I. Appelbaum, B. Huang, and D. Monsma, Nature **447**, 295 (2007).

[13] M. Morocoima, M. Quintero, E. Quintero, J. González, R. Tovar, P. Bocaranda, J. Ruiz, N. Marchán, D. Caldera, E. Calderon, J. C. Woolley, G. Lamarche, A.-M. Lamarche, J. M. Broto, H. Rakoto, L. D'Onofrio, and R. Cadenas, J. Appl. Phys. **100**, 053907 (2006).

[14] Z. V. Popović and A. Milutinović, Phys. Rev. B **73**, 155203 (2006).

[15] T. M. Pekarek, B. C. Crooker, I. Miotkowski, and A. K. Ramdas, J. Appl. Phys. **83**, 6557 (1998).

[16] A. G. Petukhov, I. Žutić, and S. C. Erwin, Phys. Rev. Lett. **99**, 257202 (2007).

[17] V. Krivoruchko, V. Tarenkov, D. Varyukhin, A. D'yachenko, O. Pashkova, and V. Ivanov, J. Magn. Magn. Mater. **322**, 915 (2010).

[18] D. A. Schmidt, T. Ohta, C.-Y. Lu, A. A. Bostwick, Q. Yu, E. Rotenberg, F. S. Ohuchi, and M. A. Olmstead, Appl. Phys. Lett. **88**, 181903 (2006).

[19] J. J. Yeh and I. Lindau, At. Data Nucl. Data Tables **32**, 1 (1985).

[20] T. Ohta, Ph.D. thesis, University of Washington, 2004.

[21] T. Lovejoy, Ph.D. thesis, University of Washington, 2010.

[22] B. Ravel and M. Newville, J. Synchrotron Rad. **12**, 537 (2005).

[23] E. N. Yitamben, T. C. Lovejoy, D. F. Paul, J. B. Callaghan, F. S. Ohuchi, and M. A. Olmstead, Phys. Rev. B **80**, 075314 (2009).

[24] G. Van der Laan and I. Kirkman, J. Phys. Condens. Matter **4**, 4189 (1992).

[25] K. W. Edmonds, N. R. S. Farley, R. P. Campion, C. T. Foxon, B. L. Gallagher, T. K. Johal, G. van der Laan, M. MacKenzie, J. N. Chapman, and E. Arenholz, Appl. Phys. Lett. **84**, 4065 (2004).

[26] S. Takatani, A. Nakano, K. Ogata, and T. Kikawa, Jpn. J. Appl. Phys., Part 2, **31**, L458 (1992).

[27] S. I. Zabinsky, J. J. Rehr, A. Ankudinov, R. C. Albers, and M. J. Eller, Phys. Rev. B **52**, 2995 (1995).

[28] A. E. Bocquet, T. Mizokawa, T. Saitoh, H. Namatame, and A. Fujimori, Phys. Rev. B **46**, 3771 (1992).

[29] T. Mizokawa, T. Nambu, A. Fujimori, T. Fukumura, and M. Kawasaki, Phys. Rev. B **65**, 085209 (2002).

[30] A. MacDonald, P. Schiffer, and N. Samarth, Nature Mater. **4**, 195 (2005).

[31] K. Lawniczak-Jablonska, R. J. Iwanowski, Z. Golacki, A. Traverse, S. Pizzini, A. Fontaine, I. Winter, and J. Hormes, Phys. Rev. B **53**, 1119 (1996).

[32] Y. Tu and J. Tersoff, Phys. Rev. Lett. **93**, 216101 (2004).

[33] K. J. Stebe, E. Lewandowski, and M. Ghosh, Science **325**, 159 (2009).

[34] Y. Wang, D. Maspoch, S. Zou, G. C. Schatz, R. E. Smalley, and C. A. Mirkin, PNAS **103**, 2026 (2006).

[35] G. M. Whitesides and B. Grzybowski, Science **295**, 2418 (2002).

[36] Q. Peng, Y. Dong, Z. Deng, H. Kou, S. Gao, and Y. Li, J. Phys. Chem. B **106**, 9261 (2002).

Figures
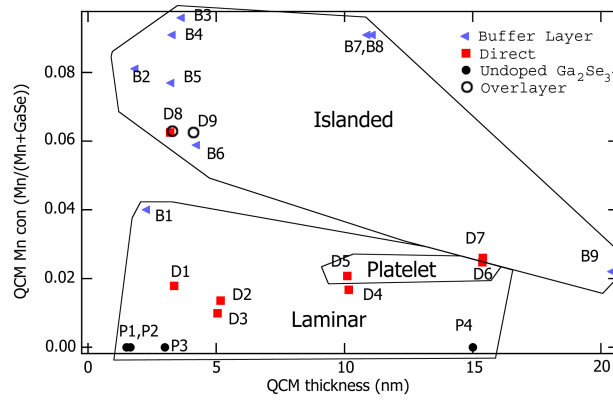
FIG. 1: (Color Online) Scatter plot showing QCM thickness and QCM Mn concentration of films grown for this study. Direct films are indicated with red boxes, buffer layer films with blue triangles, and undoped films by black dots. The grouping into laminar, platelet, and islanded is based on the morphology from STM. The labels on the samples are used throughout this article to identify specific samples.
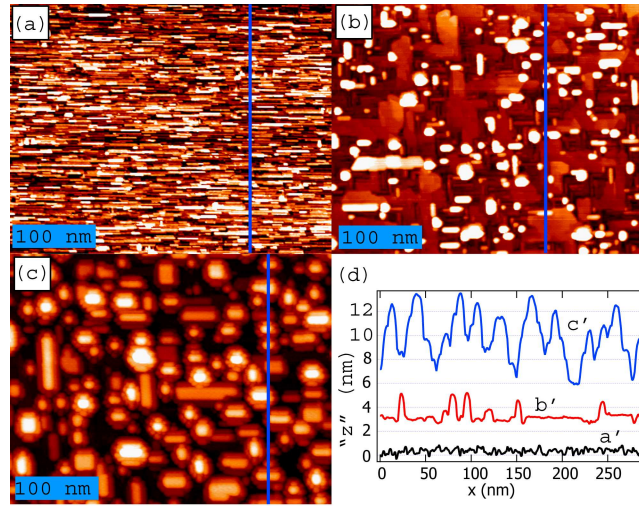
FIG. 2: STM image of direct films with QCM Mn concentration ∼2 % with increasing QCM thickness. (a, D1) 3.4 nm, (b, D5) 10 nm, and (c, D7) 15 nm. (d) line profiles through the blue lines in (a)-(c) are labeled a′–c′, respectively.

FIG. 3: STM images comparing island morphology for buffer (a, D8) and direct (b, B4) films with similar QCM thickness (∼3 nm) and QCM Mn concentration (∼ 8%). (c) and (d) are line profiles through (a) and (b), respectively.

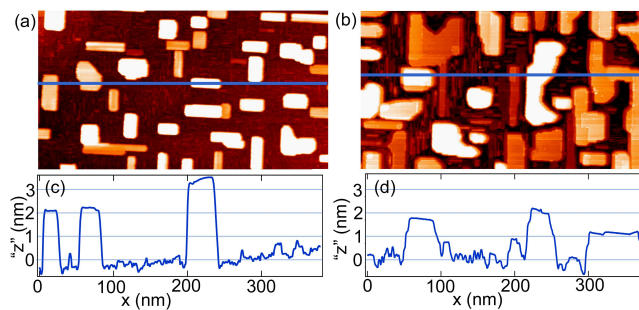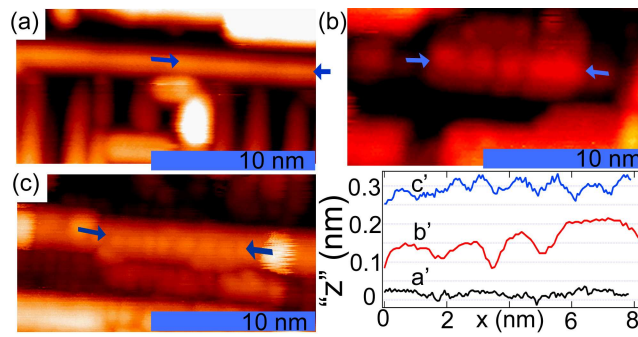FIG. 4: STM image of nanoridge morphology from (a, P2) pure Ga_2Se_3, (b, P2+Mn) 0.6 Å Mn deposited on pure Ga_2Se_3, (c, B3) the area in between the islands in a buffer layer film with QCM Mn concentration $\sim$10 %. a$'$, b$'$, and c$'$ are line profiles from between the arrows in (a), (b), and (c), respectively.
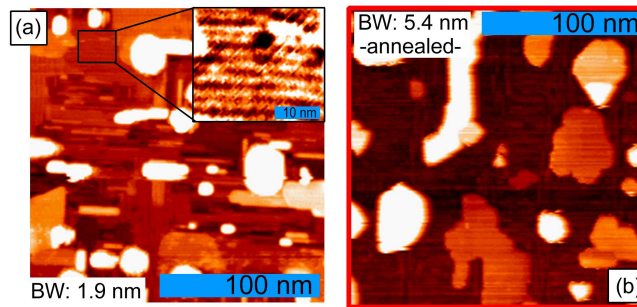
FIG. 5: STM morphology of a film with platelet morphology ($t_{QCM} \sim 15$ nm, QCM Mn con. $\sim$2%) as grown at 500 °C (a, D6). Higher resolution image of the nanoridges that make up the platelets (a inset, D6). STM morphology of the same film after annealing at 500 °C for 30 min (b, D6A)
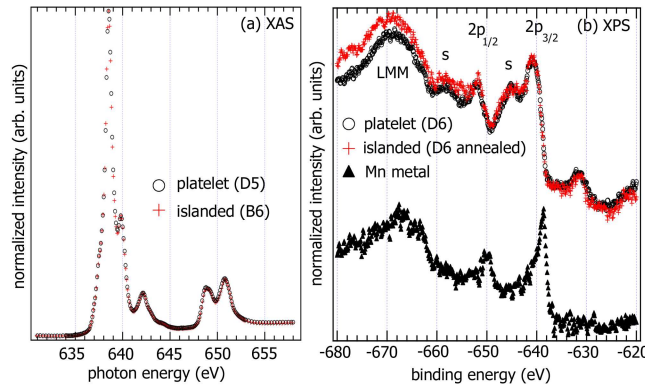
FIG. 6: (a) TEY $L_{II,III}$ edge absorption for direct Mn-doped film with platelet morphology (D5, black circles) and Mn-doped islanded film (B6, red crosses). (b) Mn 2p peak from XPS for Mn metal deposited directly on Si(001):As (black triangles), platelet morphology film D6 before (black circles) and after annealing (red crosses) at 500 °C. After annealing D6 had an islanded morphology. (see Fig. 5)
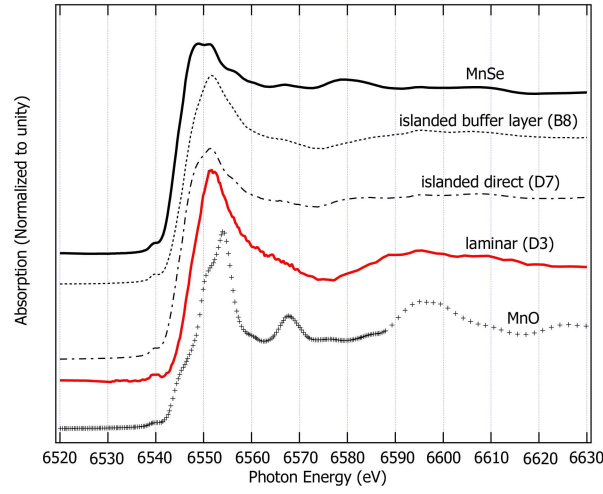
FIG. 7: (color online) Top to bottom: Mn K-edge XANES for MnSe, islanded buffer layer film (B8), islanded direct film (D7), laminar Mn-doped film (D3), and MnO reference powder.
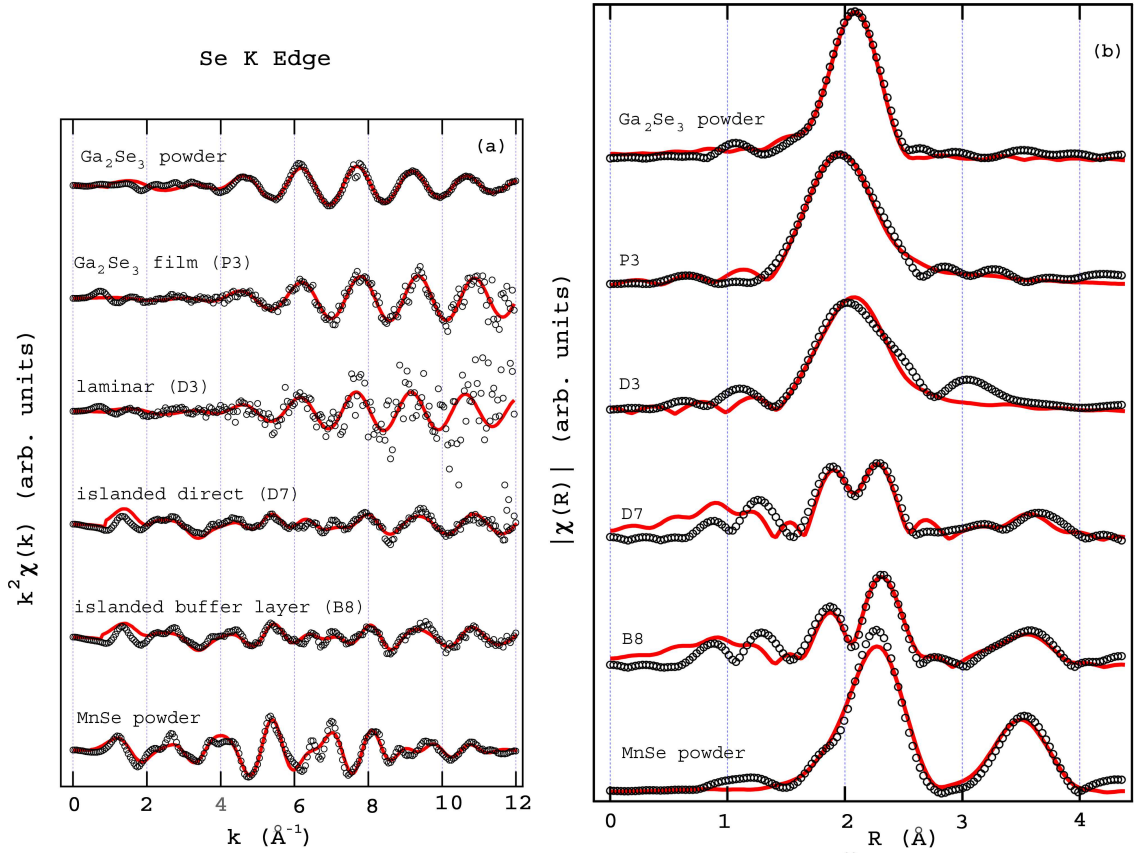
FIG. 8: (color online) Se K edge: (a) k^2 weighted $\chi(k)$ EXAFS data and (b) the magnitude of the Fourier transform, $|\chi(R)|$, for Ga_2Se_3 powder, an undoped Ga_2Se_3 film (P3), a laminar Mn-doped film (D3), an Mn-doped islanded direct film (D7), an islanded buffer layer film (B8), and MnSe powder (open circles). Fits from the FEFF6 computer program (red lines). The fit parameters are shown in Table I.

FIG. 9: (color online) Mn K-edge: (a) k^2 weighted χ(k) EXAFS data and (b) the magnitude of the Fourier transform, $|\chi(R)|$, for a laminar Mn-doped film (D3), an Mn-doped islanded direct film (D7), an islanded buffer layer film (B8), and MnSe powder (open circles). Fits from the FEFF6 computer program (red lines). The fit parameters are shown in Table I.

FIG. 10: (color online) Schematic diagram showing epitaxial relationship between Ga_2Se_3 film and MnSe islands along [110] (a) and in 3D perspective view (b). The rocksalt MnSe and defected zinc-blende Ga_2Se_3 are aligned such that the Se fcc sub-lattice continues across the interface. (Fig. from Ref.[11])

Tables

TABLE I: Se and Mn K-edge EXAFS fit parameters. Amp is the amplitude of the given component from the fit, D is fit bond length in angstroms with the statistical uncertainty in the last digit indicated in (), and σ^2 is the Debye-Waller factor from the fit. For each data set, the difference between the calculated and measured edge position was also a fit parameter (not shown). This was not allowed to vary between paths, but was varied between samples. MnSe second neighbor bond lengths were constrained to $\sqrt{2}$ times the first neighbor (nhbr) bond length. The coordination number was fixed based on the structure (2.67 for Ga_2Se_3 1st nhbr, 6 for MnSe, MnO and SeO first nhbr, and 12 for MnSe 2nd nhbr.)

	Ga_2Se_3			MnSe					Se oxide		
Se K edge	1st neighbor (Ga)			1st neighbor (Mn)			2nd nhbr. (Se)		1st neighbor (O)		
	amp	D(Å)	σ^2	amp	D(Å)	σ^2	N	σ^2	amp	D(Å)	σ^2
Ga_2Se_3 powder	0.8	2.40(2)	0.005	-	-	-	-	-	-	-	-
undoped Ga_2Se_3 film (P3)	0.5	2.34(2)	0.01	-	-	-	-	-	-	-	-

laminar, Mn-doped Ga$_2$Se$_3$ film (D3)	0.5	2.41(2)	0.002	-	-	-	-	-	-	-	-
direct, islanded Mn-doped film (D7)	0.6	2.37(2)	0.001	0.6	2.70(2)	0.02	12	0.02	0.3	1.51(2)	0.02
buffer layer, islanded Mn-doped film (B8)	0.2	2.38(2)	0.001	0.4	2.70(2)	0.01	12	0.01	0.4	1.52(4)	0.03
MnSe powder	-	-	-	0.9	2.71(1)	0.01	12	0.01	-	-	-

Mn K edge				MnSe					Mn oxide		
				1st neighbor (Se)			2nd nhbr. (Mn)		1st neighbor (O)		
laminar, Mn-doped Ga$_2$Se$_3$ film (D3)	-	-	-	-	-	-	-	-	0.7	2.12(7)	0.01
direct, islanded Mn-doped film (D7)	-	-	-	0.3	2.72(2)	0.008	12	0.02	0.2	2.17(2)	0.004
buffer layer, islanded Mn-doped film (B8)	-	-	-	0.5	2.70(1)	0.01	12	0.02	0.2	2.13(3)	0.008
MnSe powder	-	-	-	0.7	2.70(1)	0.01	12	0.02	-	-	-